International Journal of Engineering

Development of a New Supersonic Rotor-vane Ejector using Computational Fluid Dynamics

M. Sarvalishah, S. Niazi*, Y. Bakhshan

Department of Mechanical Engineering, University of Hormozgan, Bandar Abbas, Iran

P A P E R   I N F O

A B S T R A C T

An innovative design of a supersonic rotor pressure-exchange ejector is introduced in this paper. In this design, momentum is exchanged between supersonic primary flow and secondary flow using an idle rotor. A CFD code developed to model the 3-D compressible, viscous and turbulent flow of air inside the new design of ejector. Roe approach and Spallart-Allmaras methods used to analyze flow inside the ejector. The flow inside the ejector was modeled by using a structured grid and air was employed as the working fluid in both primary and secondary streams. The Mach number of the motive flow was set at 2. Momentum exchanged between the primary and secondary flows because of direct contact between those. In addition to that, rotation of idle rotor and mechanical blades entrained the secondary flow to the ejector. Enthalpy, entrained mass flow rate and created vacuum presented for the flow inside the ejector for different configurations of the rotor and ejector until an optimum case was achieved. Also, uniformity of the flow at discharge section compared between ejectors. For the optimum case with the presented geometry, the ultimate rotor speed of 50000 rpm was obtained and an increase of 47% in entrainment ratio achieved with respect to the stationary blades. To study the flow field in more details, the contours of the Mach number and stagnation pressure were compared according to the different sections of computational domain.

doi: 10.5829/ije.2021.34.01a.26

NOMENCLATURE

Q	Primitive variable matrix	e	Total energy per unit mass
E, F, G	Inviscid fluxes	q_i	Heat flux
E_v, F_v, G_v	Viscous stresses and heat fluxes	**Greek Symbols**	
x, y, z	Cartesian coordinates	ρ	Density
t	Time	τ_{ij}	Viscous stress tensor
u, v, w	Cartesian velocity components	v	Kinematic viscosity
p	Pressure	v_t	Turbulent viscosity
W_{ij}	Vorticity tensor	$\bar{v}$	Working variable in Spalart-Allmaras turbulence model
d	Distance from nearest wall	Ω	Magnitude of vorticity

1. INTRODUCTION

Ejectors are widely used in different industries. This device can convert low-grade energies into power. In addition to the ability of creating compression without using any moving parts, ejectors have the advantage of a simple structure causing their manufacturing,

installations and operations to be simpler than those of other compression systems.

One of the major applications of ejectors is in Ejector Refrigeration Systems (ERS). Le Blanc and Parson developed the first steam jet refrigerator in the early 1900s. It has experienced great popularity during the early 1930s for the air conditioning systems of large buildings. Ejectors are also utilized in vacuum systems

*Corresponding Author Institutional Email: s.niazi@hormozgan.ac.ir (S. Niazi)

like steam surface condensers. In this way, ejector reduces the pressure and temperature in condenser and therefore, smaller sizes of condensers can be employed to perform the same duty of condensation. Moreover, ejectors are also applied for evacuation of vessels containing toxic or flammable gases.

The streams passing through ejectors include high and low energy streams in which a high pressure flow is converted into a high speed flow after passing through the convergent-divergent motive nozzle of an ejector. This flow entrains a secondary flow through the suction nozzle and after exchanging power and mixing high and low energy streams in the mixing chamber, there will be an intermediate pressure in the discharge nozzle. In other words, ejectors can entrain a secondary flow and increase its pressure through a high energy flow at the primary nozzle.

In spite of all the benefits of ejectors, they have low efficiencies. Therefore, many researches are being conducted on ejectors to improve their efficiencies and entrainment ratios. Some of these studies are reported hereunder.

Suvarnakuta et al. [1] have used the computational fluid dynamics (CFD) to investigate the performance of a steam ejector employed in a refrigeration system to increase its functionality and coefficient of performance (COP). They modeled a 2D-axisymmetric two stage ejectors and performance compared with the available single stage ejector refrigeration system. CFD results provided high entrainment ratio of 77.2% and 21.9% decrease in back pressure of ejector system. In this research, they achieved high refrigeration capacity and low condensing pressure.

Meyer et al. [2] established an experimental setup of a small-scale steam jet ejector. They studied the Coefficient of Performance (COP) of their ejector with changing the primary and secondary throat diameters, boiler temperature, motive nozzle discharge position and condenser pressure.

XChen et al. [3] provided a literature review on the recent development of ejectors and refrigeration systems. They reported several useful researches in their review articles, including refrigerant selections, mathematical modeling and numerical simulation of ejector systems, geometric optimizations, modification of operating conditions and combinations with other refrigeration systems.

Hong et al. [4] presented a computational and experimental program for designing a rotor-vane/pressure-exchange ejector for thermally driven ejector refrigeration systems. In their research, careful management was performed to control the entropy rise through the oblique shocks and boundary layers. They focused on the selection, design and optimization of their ejector rotor and blades. In addition, total pressure distribution for different blade spin angles and different rotor speeds were compared.

Gould and Garris [5] worked on the computer simulation and theoretical analysis of a steam pressure exchange ejector for an automobile. Waste heat from the internal combustion engine exhaust was captured to run the boiler of the steam ejector refrigeration system. In their study, theoretical and numerical results compared with the experimental data from an existing ejector refrigeration system for the automobile.

Chenghua et al. [6] used CFD methods to study the entropy production and pressure loss in a supersonic rotor-vane ejector. The expansion shock waves at the rotor tails induced the secondary flow and enhanced the mixing of two flows at a short distance. They showed that turbulence effects were weak and negligible. They had also studied effects of vane configuration and speed on ejector efficiency.

2. TURBO-EJECTOR

To resolve the problem of low efficiency and small entrainment ratio in ejectors, a new configuration was presented for them. In this configuration, an integrally turbine-compressor blade was located in front of the primary flow. In fact, the rotor blades played the roles of both turbine and compressor blades. Figure 1 shows a schematic view of the desired turbo-ejector. In this model, a high pressure-flow enters the motive nozzle and expands to supersonic speed after passing through the convergent-divergent primary nozzle.

Same as the turbine, admission of the high-velocity flow to the inner part of the blades caused the cascade to rotate around the frictionless shaft. Thus, the outer part acted as a compressor blade and entrained the flow from the suction chamber. In this way, two different natures of flow entrainment were employed. The first was the shear stresses at the tangential interface between the primary and secondary flows as a result of turbulence and viscosity, and the work of normal pressure forces. This is the same scenario that appears in common ejectors. The second was the solid vanes that transferred momentum
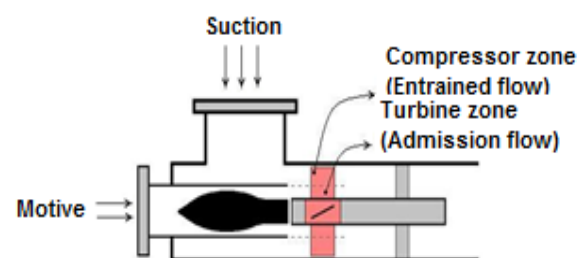

Figure 1. A schematic view of turbo-ejector

and energy to the fluid in contact, like the turbo-machines.

In this study, a CFD code named HORMOZ 3-D was developed for analyzing and modeling 3-D turbulent compressible flow inside the introduced turbo-ejector.

3. GOVERNING EQUATIONS

To model the flow inside the turbo-ejector, the system of partial differential equations for the conservation of mass, momentum and energy, known as the Navier-Stokes equations, were employed. The complex nature of the governing equations limits the analytical solutions to simple flows and configurations. Therefore, numerical techniques are required for more complex problems. The control volume procedure used in Roe's method [7, 8, 9] was applied to model a three-dimensional compressible flow inside the turbo-ejector. The Spalart-Allmaras method was also employed with some modifications to model the turbulent flow inside the domain [10].

In the three-dimensional Cartesian coordinates, the conservative form of the equations is given in a vector form as follows:

$$Q_t + (E - E_v)_x + (F - F_v)_y + (G - G_v)_z = 0 \qquad (1)$$

where Q is the primitive variable matrix, t time and x, y, z are the three directions in the Cartesian coordinate. Matrices E, F and G are inviscid flux terms, and E_v, F_v and G_v represent viscous terms. Matrix Q and inviscid flux terms are:

$$Q = \begin{Bmatrix} \rho \\ \rho u \\ \rho v \\ \rho w \\ \rho e \end{Bmatrix}, E = \begin{Bmatrix} \rho u \\ \rho u^2 + p \\ \rho uv \\ \rho uw \\ \rho(e + \frac{p}{\rho})u \end{Bmatrix},$$

$$F = \begin{Bmatrix} \rho v \\ \rho uv \\ \rho v^2 + p \\ \rho vw \\ \rho(e + \frac{p}{\rho})v \end{Bmatrix}, G = \begin{Bmatrix} \rho w \\ \rho uw \\ \rho vw \\ \rho w^2 + p \\ \rho(e + \frac{p}{\rho})w \end{Bmatrix} \qquad (2)$$

where e is total energy per unit mass.

The viscous terms are:

$$E_v = \begin{Bmatrix} 0 \\ \tau_{xx} \\ \tau_{xy} \\ \tau_{xz} \\ u\tau_{xx} + v\tau_{xy} + w\tau_{xz} - q_x \end{Bmatrix},$$

$$F_v = \begin{Bmatrix} 0 \\ \tau_{yx} \\ \tau_{yy} \\ \tau_{yz} \\ u\tau_{yx} + v\tau_{yy} + w\tau_{yz} - q_y \end{Bmatrix}, \qquad (3)$$

$$G_v = \begin{Bmatrix} 0 \\ \tau_{zx} \\ \tau_{zy} \\ \tau_{zz} \\ u\tau_{zx} + v\tau_{zy} + w\tau_{zz} - q_z \end{Bmatrix}$$

General form of the Spalart-Allmaras turbulence model with the assumption of turbulence flow at the entrance to the blades is:

$$\frac{D\bar{v}}{Dt} = C_{b1}\bar{\Omega}\bar{v} + \frac{1}{\sigma}\left[\nabla.\left((v + \bar{v})\nabla\bar{v} + C_{b2}(\nabla\bar{v})^2\right)\right] - C_{w1}f_w\left[\frac{\bar{v}}{d}\right]^2 \qquad (4)$$

where turbulent kinematic viscosity is:

$$v_t = \bar{v}f_{v1}, f_{v1} = \frac{X^3}{X^3 + C_{v1}{}^3}, X = \frac{\bar{v}}{v} \qquad (5)$$

and

$$\bar{\Omega} = \Omega + \frac{\bar{v}}{K^2 d^2}f_{v2}, f_{v2} = 1 - \frac{X}{1 + Xf_{v1}},$$

$$f_w = g\left[\frac{1 + C_{w3}{}^6}{g^6 + C_{w3}{}^6}\right]^{1/6}, g = r + C_{w2}(r^6 - r), \qquad (6)$$

$$r = \frac{\bar{v}}{\bar{\Omega}K^2 d^2}, \Omega = \sqrt{2W_{ij}W_{ij}}$$

W_{ij} is the vorticity tensor. To solve the equation, $\bar{v}$ was set to zero for the wall boundary conditions. Other constant parameters were set as below:

$$\sigma = 2/3, C_{b1} = 0.1355, C_{b2} = 0.622,$$

$$K = 0.41, C_{w1} = \frac{C_{b1}}{K^2} + \frac{(1 + C_{b2})}{\sigma}, C_{w2} = 0.3, C_{w3} = 2, C_{v1} = 7.1 \qquad (7)$$

As stated before, one of the major roles of ejectors is to transfer power from high-energy (motive) zone to the low-energy (suction) zone. In other words, it is favorable to have a uniform distribution of stagnation enthalpy at the discharge section. To count the uniformity, two parameters of $H_{0,outlet}$ (summation of stagnation enthalpy at the discharge section) and $H_{0,non-uniformity}$ (summation of enthalpy deviation from the average value) are defined as follows:

$$H_{0,outlet} = \left(\sum \dot{m}C_p T_0\right)_{outlet\ section} \qquad (8)$$

$$H_{0,non-uniformity} = \sum \dot{m}\left(\frac{H_{0,outlet}}{\dot{M}_{outlet}} - C_p T_0\right)_{outlet\ section} \qquad (9)$$

The above equations were employed to compare the enthalpy distribution in different turbo-ejector models. It is also noticeable that the above mentioned stagnation enthalpies were based on the absolute velocities in the ejector.

Entrainment ratio is defined as:

$$Entrainment\ ratio = \frac{\dot{M}_{suction\ zone}}{\dot{M}_{motive\ zone}} \qquad (10)$$

where $\dot{m}$ and $\dot{M}$ are mass flow rates at each cell and at the specified section, respectively.

Navier-Stokes equations were written in the Rotating Reference Frame (RRF) for both stationary and moving parts. Explicit discretization was used for Navier-Stokes equations and turbulence modeling.

For the code validation, the experiment results of some internal and external flows were compared with the code solutions. Also, convergence history and grid independency were reviewed and checked for the solutions achieved from this code.

4. TURBO-EJECTOR GEOMETRY

To analyze the flow in turbo-ejectors, the domain between two adjacent blades, including inlet and outlet zones, was chosen as shown in Figure 2. A structural grid with the dimensions of $105 \times 40 \times 40$ in X, Y and Z directions was employed as displayed in the following figure (Figure 2).

In this research, the following geometries were analyzed and studied for the flow inside the turbo-ejector. Rotor had the inner and outer blade diameters of 6 cm and 10 cm, respectively with the width of 2 cm. The lengths of the stationary zone at the blade upstream and downstream were 1cm and 5cm, respectively. The blade orientations with respect to the rotation axis were $10°$ and $20°$ and the flow direction at the entrance was in the positive X direction which is the rotation axis. Figure 3 represents a schematic view of four turbo-ejector rotors with different configurations.

All these rotors were located in the ejectors with similar configurations and some comparisons were made between those to find the best solution for the turbo-ejector.

5. CODE VALIDATION

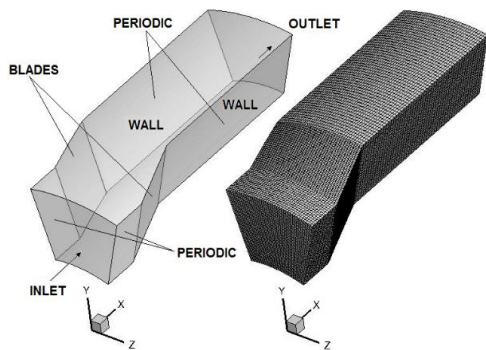To validate the in-house developed code, grid independencies were checked for different cases and the

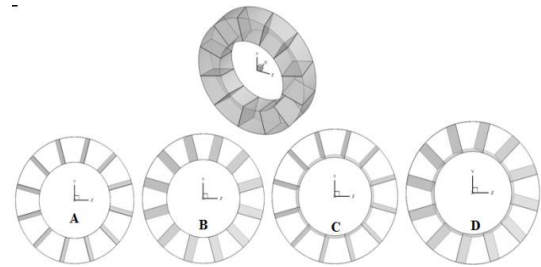**Figure 2.** Computational domain of ejector and the structured grid

Figure 3. A schematic 3-D and 2-D views of four rotors with different configurations
A: Pitch angle 10°; B: Pitch angle 20°; C: Pitch angle 10° with conical hub angle of 28°; D: Pitch angle 20° with conical hub angle of 28°

same results achieved for pressure, density, temperature and velocity components in the flow field. In addition, graphs of convergence history depicted the smooth convergence of the code to the final solutions. As a sample, convergence history for Ejector B is represented in Figure 4, where the vertical axis (Error) is the difference between two alternative iterations for the summation of the desired parameter in the whole domain and the axial axis is the number of iterations.

As shown here, this case is converged in less than 30000 iterations for the grid dimensions of $105 \times 40 \times 40$ in X, Y and Z directions.

In addition to above, this code was checked and proved for some other internal and external flows. A sample is shown in Figure 5 that is the supersonic flow on a cone with different attack angles [11].

Mach number for air at the entrance to the cone was 2.72 and as shown in Figure 6, a structured grid with the dimensions of $30 \times 70 \times 20$ in axial, radial and circumferential directions was employed.

Figure 7 shows the results for pressure coefficient on the cone body in circumferential direction for the various angles of attack as $a = 0°{\sim}30°$.

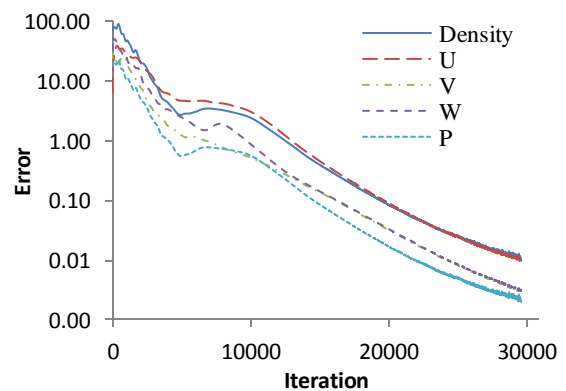Results showed acceptable conformity of experimental and numerical results.

Figure 4. Convergence history of the flow in Ejector B
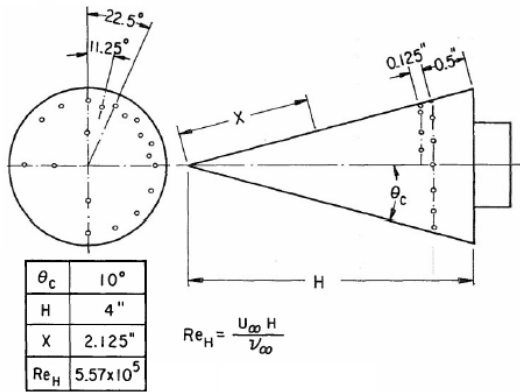
Figure 5. Cone geometry and the location of pressure probes
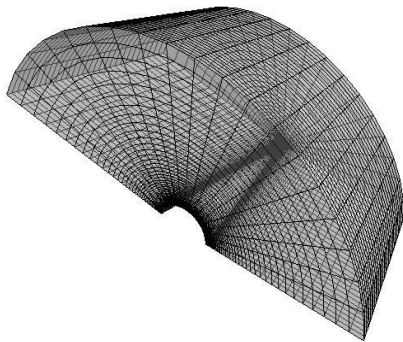

Figure 6. Structured grid on the cone with dimensions of $30 \times 70 \times 20$ in axial, radial and circumferential directions
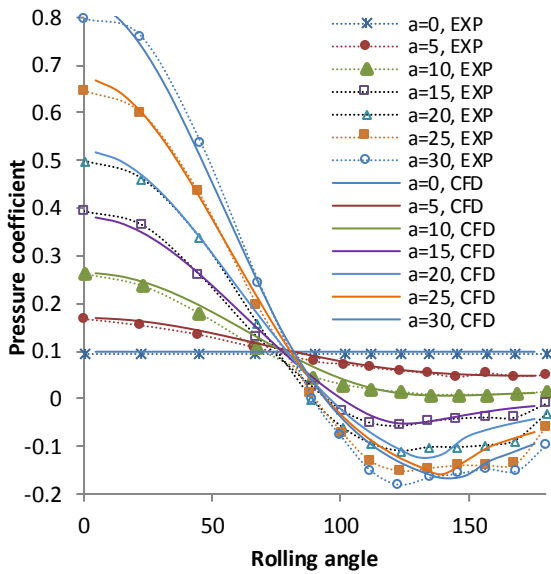

Figure 7. Circumferential pressure distribution for the cone at various angles of attack

Generally, results for grid independency, convergence history and different case studies depicted the acceptable solutions of this code.

6. BOUNDARY CONDITIONS

Air was the working fluid for both the admitted and entrained sections of the ejector. Mach number at the entrance to the admission zone was 2 with the static pressure and temperature of 100KPa and 300K, respectively. The stagnation pressure and temperature at the entrance to the entrained part of the turbo-ejector were 100KPa and 300K, respectively. The one-dimensional Riemann characteristic equation was used to find the entrained flow velocity [12, 13]. For the outlet section, the supersonic flow parameters were extrapolated from the properties inside the domain and back pressure of 100Kpa was set for the subsonic region. Periodic boundary conditions were considered for the side walls of the inlet and outlet zones and no slip condition was set for the flow on the blade walls.

7. RESULTS

In this part, all Ejectors A, B, C and D were analyzed and flow parameters compared between ejectors. Then, the best case was chosen to study the flow field in more details. High energy admission to the ejector caused the rotor to reach its final speed when began to rotate idly around its axis. To find the final speed using CFD analysis, the speed was increased from zero and the resultant momentum on the rotor in axial direction (rotation axis) was calculated in each stage. The final speed occurred when the resultant momentum on the rotor equaled zero. Figure 8 shows a sample of momentum variation with regard to the rotor speed for Ejector B. As shown in this figure, final speed of 50000 rpm was achieved, where axial momentum on the rotor became zero.

Figure 9 shows the variations of enthalpy non-uniformity, $H_{0,non-uniformity}$, with regard to the rotor speed for all the ejectors. In this diagram, speed increased from zero to the final speed of ejector.
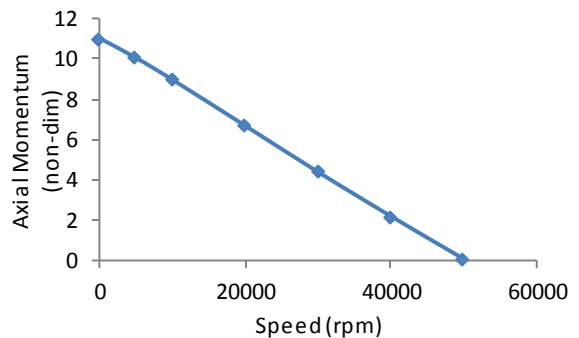

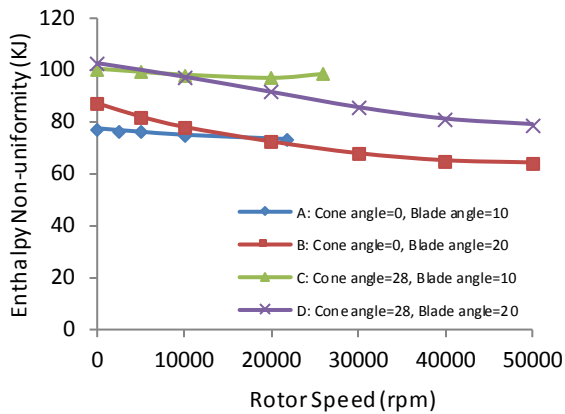**Figure 8.** Variations of the torque on the rotor of ejector B with respect to its speed

Figure 9. Variation of stagnation enthalpy non-uniformity for the ejectors with respect to the rotor speed

Figure 11. Variation of suction static pressure for the ejectors with respect to the rotor speed

As shown in this figure, non-uniformities for Ejectors A and B are less than Ejectors C and D. In other words, Ejectors A and B have more uniform distributions of stagnation enthalpy at the outlet section compared to those of Ejectors C and D. Also, Ejector B displayed a slightly better operation than Ejector A.

One of the modifications on ejectors is to suction more flow through suction nozzle and to create more vacuum in this region. Figures 10 and 11 represent and compare the mass flow rate and suction pressure in entrained region between different configurations of ejectors.

As shown in Figure 10, the highest entrained flow appears in Ejector B. It is such that the motive mass flow rates are the same for all ejectors. Results show that mass flow rate for Ejectors A and B are higher than those for C and D. This means that conical hub and created oblique shock wave has reduced the entrained mass flow rate through suction zone.

Suction pressure in the region of entrained flow is presented and compared for all ejectors in Figure 11.
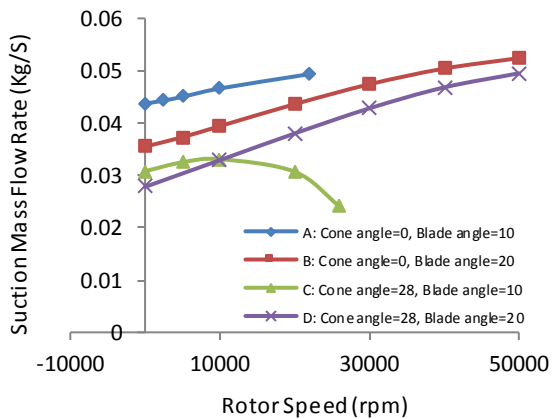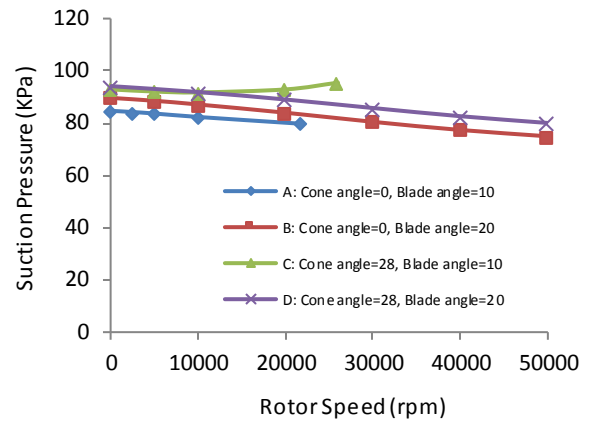
As shown in this figure, the same as previous results, Ejectors A and B have created higher vacuum (lower suction pressure) with respect to Ejectors C and D.

Entrainment ratio of Ejectors for speed variations from zero to final speed is prototyped in Figure 12.

As shown in this figure, increase in rotor speed and blade rotation cause enhancement of the entrainment ratio. It means that mass flow rate in suction side of the ejector increases by raising the rotor speed from zero to the final speed. As a sample for Ejector B, the entrainment ratio was 0.36 for the rotor final speed of 50000 rpm. It is such that, an increase of 47% in entrainment ratio achieved with respect to the stationary blades of this ejector.

All above results obtained in Figures 9, 10, 11 and 12 prove that Ejector B has shown better results than other ejectors. Thus, the CFD results of Ejector B were focused on.

To study the ejector in more details, some sections depicted in Figure 13 were selected for reporting flow properties inside the domain.
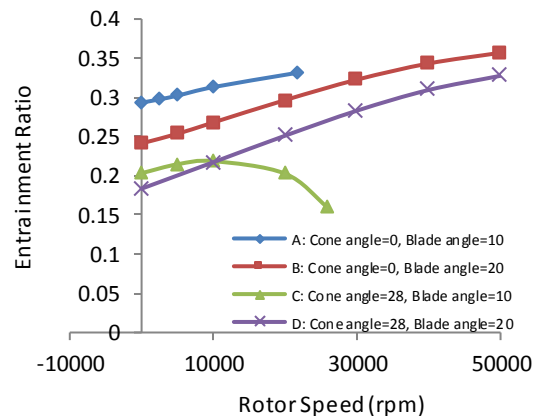

Figure 10. Variation of suction mass flow rate for the ejectors with respect to the rotor speed

Figure 12. Entrainment ratio variations with respect to the rotor speed for all ejectors
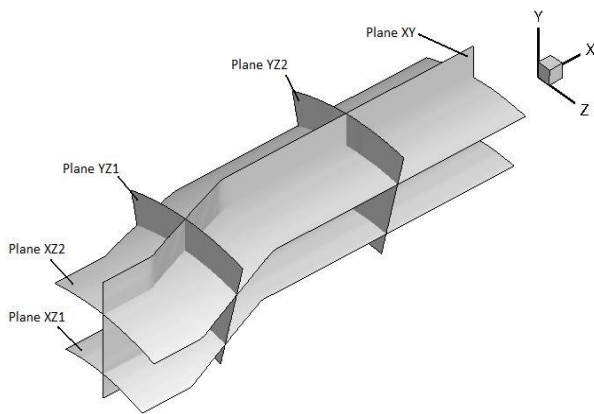
Figure 13. A schematic view of some selected sections

Figure 15. Contours of Mach number on Planes XZ1 and XZ2 inside the domain

As can be seen, Plane XY is located at the middle of the domain in axial direction. Planes XZ1 and XZ2 are at middles of admission domain and suction zone in radial direction, respectively. In the same manner, Planes YZ1 and YZ2 are at the middles of the blade section and discharge zone in circumferential direction, respectively.

In Figure 14, the streamlines on some planes are displayed based on the absolute velocities. As shown in this figure, the secondary flows appear in the blade and discharge zones in the axial direction. These secondary flows can mix the high and low energy streams in the flow field and improve the uniformity of enthalpy at the discharge section. In addition, there is a tendency of the motive flow to expand towards the suction zone on Plane XY.

The contours of the absolute Mach number on two different planes in the axial direction are prototyped in Figure 15. Creations of the oblique shock waves at the edges of the blades in the admission zone are shown in Plane XZ1. As can be seen in plane XZ2 that is located in the entrained zone, Mach number increases gradually from the inlet to the outlet section of the ejector.

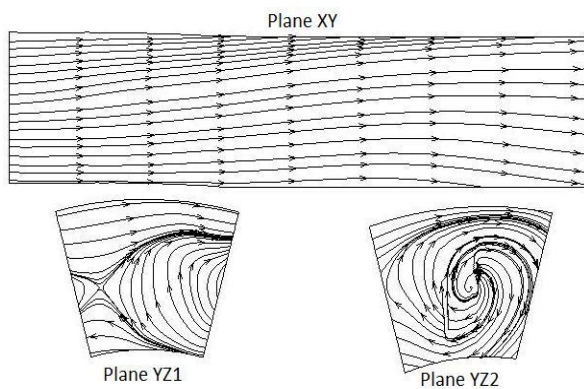However, as shown in this figure, there are some secondary flows that are mixing the primary and

secondary streams at the downstream of the blades. The detailed contours of Mach number on Plane XY are shown in Figure 16. Mach number at the entrance to the ejector is 2 for motive flow and nearly 1 for the suction flow. The secondary flows are also shown at the downstream of the blade. In this figure the contour of Mach number for the rotor with zero speed is compared with its final speed. As shown, the Mach number of the entrained flow at the inlet to the ejector is about 0.4 for Plane XY in the second case when the rotor is fixed. In a way that same value of about 1 has been obtained for the rotor final speed of 50000 rpm. In other words, rotation of the blades has increased the Mach number of the entrained stream to the sonic flow and thus, a higher entrainment ratio has been achieved.

Counters of the stagnation pressure on three sections of the inlet, outlet and Plane XY are displayed in Figure 17. This figure shows the variation of total pressure through ejector. Contours of P_0 in the inlet section represent the huge difference between momentums of the motive and suction flows. Similar results for Plane XY indicate the momentum exchange between the high and low energy streams when passing through the turbo-ejector.
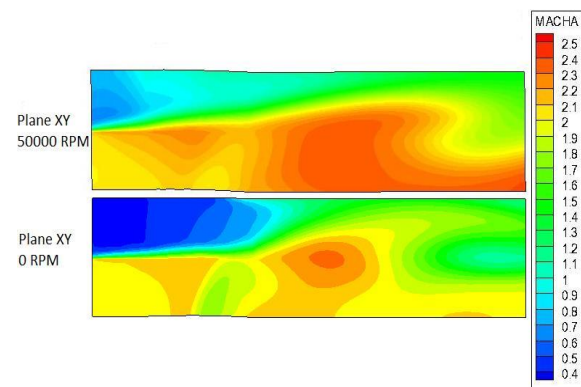

Figure 14. Streamlines on the planes XY, YZ1 and YZ2

Figure 16. Contours of Mach number on Plane XY inside the domain the for stationary and rotating blades
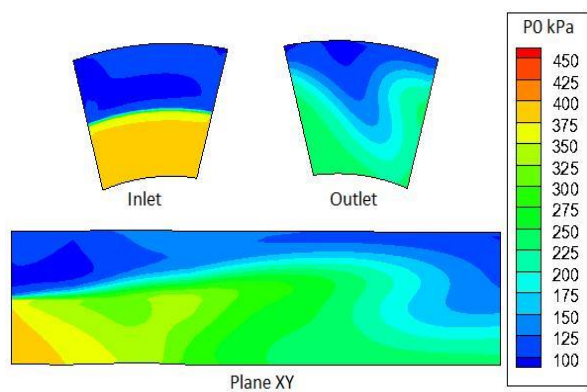
Figure 17. Contours of stagnation pressure on planes XY, inlet and outlet

P_0 distribution is also depicted in the outlet section of the ejector. Comparison between inlet and outlet sections shows the momentum exchange between primary and secondary flows. However, the flow at the discharge is not uniform and more power exchange can occur at the downstream of the ejector.

8. CONCLUSION

In this investigation, a new configuration has been presented for an ejector equipped with an idle rotor. To analyze the flow inside the rotor, a CFD code of HORMOZ 3-D was developed to model the 3-D compressible, viscous and turbulent flow. Four ejectors with different rotor configurations were modeled and the best case was selected to study the flow in more detail. Entrainment ratio variations with respect to the rotor speed were reported for the ejectors. The rotor speed ramped to the final speed where the torque on the rotor was zero and a speed of 50000 rpm was achieved for Ejector B. At this speed, the streamlines and contours of Mach number and stagnation pressure on different sections of the flow field were examined. The contours clearly revealed the creations of compression and expansion oblique shock waves. Results indicated that motive flow at the outlet of the ejector, still have more power to be exchanged with the entrained flow, while some further exchange power could occur downstream of the rotor to provide better efficiencies. In addition, higher efficiencies could result from rotor geometry optimization.

9. REFERENCES

1. Suvarnakuta, N., Pianthong, K., Sriveerakul, T., & Seehanam, W.," Performance analysis of a two-stage ejector in an ejector refrigeration system using computational fluid dynamics", *Journal of Engineering Applications of Computational Fluid Mechanics*, Vol. 14, (2020), 669-682, doi: 10.1080/19942060.2020.1756913

2. Meyer, A. J., Harms, T. M., Dobson, R. T., "Steam jet ejector cooling powered by waste or solar heat", *Journal of Renewable Energy*, Vol. 34, (2009), 297-306, doi: 10.1016/j.renene.2008.03.020

3. Chen, X., Omer, S., Worall, M., Riffat, S., "Recent Developments in ejector refrigeration technologies", *Journal of Renewable and Sustainable Energy Reviews*, Vol. 19, (2013), 629-651, doi: 10.1016/j.rser.2012.11.028

4. Hong, W. J., Alhussan, Kh., Zhang, H., Garris, C. A., "A novel thermally driven rotor-vane/pressure-exchange ejector refrigeration system with environmental benefits and energy efficiency", *Journal of Energy*, Vol. 29, (2004), 2331-2345, doi: 10.1016/j.energy.2004.03.050

5. Gould, D., Garris, C., "Theoretical analysis of the pressure exchange ejector for an automotive car conditioning applications", George Washington University, Master of Science thesis, (2009).

6. Chenghua, C., Qiang, P., Xingyou, Y., & Juan, Z., "Numerical simulation of flow mechanism of unsteady supersonic rotor-vane ejector", *Journal of High Power Laser and Particle Beams*, Vol. 26, (2014), 039001, doi: 10.2514/6.2001-858.

7. Chackravarthy, S. R., Szema, K. Y., "Euler Solver for Three-Dimensional Supersonic Flows with Subsonic Pockets", *Journal of Aircraft*, Vol. 24, No. 2, (1987), 73-83.

8. Farhanieh, B., Amanifard, N., Ghornanian, K., "Numerical Investigation on Compressible Flow Characteristics in Axial Compressors Using Multi-Block Finite Volume Scheme", *International Journal of Engineering, Transactions A: Basics*, Vol. 15, (2001), 91-104.

9. Bagheri-Esfe, H., Dehghan Manshadi, M., "A Low Cost Numerical Simulation of a Supersonic Wind-tunnel Design", *International Journal of Engineering, Transactions A: Basics*, Vol. 31, No. 1, (2018), 128-135, doi: 10.5829/ije.2018.31.01a.18

10. Allmaras, S. R., Johnson, F. T., Spalart, P. R., "Modification and Clarification for the Implementation of the Spalart-Allmaras Turbulence Model", 7th international conference on Computational Fluid Dynamics, Big Island, Hawaii, (July 9-13, 2012), 2012.

11. R. Yahalom, "An experimental investigation of supersonic flow past yawed cones", College of engineering, University of Calofornia, Berkeley, Report No. AS-71-2, (1971).

12. Adel Zaki, M., "Physics Based Modeling of Axial Compressor Stall", Georgia Institute of Technology, PHD thesis, (2009).

13. Niazi, S., "Numerical Simulation of Rotating Stall and Surge Alleviation in Axial Compressors", Georgia Institute of Technology, PHD thesis, (2000).

Persian Abstract

چکیده

در این تحقیق یک طرح جدید از اجکتور پرهدار فراصوتی ارائه شده است که در آن از یک روتور هرزگرد برای انتقال ممنتم از جریان فراصوتی اولیه به جریان ثانویه کمک گرفته شده است. برای بررسی و مدلسازی جریان درون این نوع اجکتور یک کد CFD تولید شده است که قادر است جریان سهبعدی، تراکمپذیر، گرانرو و متلاطم را درون اجکتور شبیهسازی کند. در این کد از روش Roe و مدل تلاطمی Spallart-Allmaras برای مدلسازی جریان تراکمپذیر و متلاطم درون اجکتور استفاده شده است. برای این کار از یک شبکهی سازمانیافته استفاده شده و هوا به عنوان جریان اولیه و ثانویه به کار گرفته شده است. عدد ماخ هوا در خروجی نازل جریان اولیه و در ورودی به پره های روتور ۲ میباشد. این جریان علاوه بر این که با جریان ثانویه در تماس است و انتقال ممنتم از طریق تماس آنها رخ می دهد، سبب چرخش روتور هرزگرد نیز میشود که در پی آن جریان ثانویه به کمک پرههای مکانیکی به درون اجکتور مکیده میشود. در این تحقیق چندین هندسه متفاوت از اجکتور بررسی شده و میزان آنتالپی، جریان مکش شده و فشار مکش برای حالتهای مختلف مقایسه شده است. همچنین، معیاری برای مقایسه و اندازهگیری میزان یکنواختی جریان در خروجی از اجکتورها ارائه شده است. طبق نتایج به دست آمده در بهترین حالت از گزینههای مورد بررسی، سرعت روتور ۵۰۰۰۰ دور بر دقیقه بوده و نسبت مکش در مقایسه با همان اجکتور با روتور ثابت، ٤٧٪ افزایش نشان میدهد. برای بررسی جریان با جزئیات بیشتر، کانتورهای ارائه شده میزان تغییرات عدد ماخ و فشار کل را در مقاطع و صفحات مختلف از اجکتور نشان میدهد.